LBL-32591
UC-401
Preprint

Lawrence Berkeley Laboratory
UNIVERSITY OF CALIFORNIA

# CHEMICAL SCIENCES DIVISION

Submitted to Journal of Chemical Physics

## Vibration-Rotation Spectroscopy of the Hydrated Hydronium Ions $H_5O_2^+$ and $H_9O_4^+$

L.I. Yeh, Y.T. Lee, and J.T. Hougen

June 1992

Prepared for the U.S. Department of Energy under Contract Number DE-AC03-76SF00098

## DISCLAIMER

LBL-32591
UC-401

# Vibration-Rotation Spectroscopy of the Hydrated Hydronium Ions $H_5O_2^+$ and $H_9O_4^+$

L.I. Yeh* and Y.T. Lee

Department of Chemistry
University of California

and

Chemical Sciences Division
Lawrence Berkeley Laboratory
University of California
Berkeley, California 94720

and

J.T. Hougen

Molecular Physics Division
National Institute of Standards and Technology
Gaithersburg, Maryland 20899

June 1992

*Present Address: Exxon Research and Engineering Company
Annadale, New Jersey 08801

This work was supported by the Director, Office of Energy Research, Office of Basic Energy Sciences, Chemical Sciences Division, of the U.S. Department of Energy under Contract No. DE-AC03-76SF00098.

## ABSTRACT

High resolution vibration-rotation spectra in the OH antisymmetric stretching region near 3700 $cm^{-1}$ are reported for $H_5O_2^+$ and $H_9O_4^+$. The clusters are produced in a corona discharge ion source, cooled by supersonic expansion, mass-selected and trapped in an RF octopole ion trap. Spectroscopic interrogation using a two-color laser scheme leads to rovibrational excitation of the trapped ions followed by preferential multiphoton dissociation of the vibrationally excited ions and detection of the resultant fragment ions. Many more lines appear in the partially resolved vibration-rotation spectrum of $H_5O_2^+$ than can be explained if the molecule is rigid, and we have assumed that these additional lines arise from tunneling splittings caused by large-amplitude internal motions in this ion. Despite the low signal-to-noise ratio, all the observed spectral features can be grouped into roughly twelve R branches with a line spacing only 14% less than the B+C value calculated from the ab initio structure. Theoretically expected splitting patterns were calculated using a formalism developed earlier for tunneling motions in hydrazine, since $H_2N\text{-}NH_2$ and $H_2O\text{-}H^+\text{-}OH_2$ are group-theoretically similar if the central proton of the ion is located symmetrically between the two water molecules. We tentatively conclude that the twelve branches represent the overlapping of six tunneling-split components for the in-phase and six for the out-of-phase OH antisymmetric stretching vibrations expected in this region, but the low signal-to-noise ratio in the present measurements prevented unambiguous comparison of theory and experiment.

## Introduction

Recent progress in the field of infrared ion spectroscopy has been impressive. Despite low ion densities and the presence of many species related to the one under study, high resolution infrared spectra of rigid simple positive and negative ions have been obtained using direct laser absorption for over 60 species.[1] The next challenge to ion spectroscopists is to obtain spectra of cluster ions and other floppy ions. This has been achieved in the last few years under low resolution for several series of cluster ions, including the hydrogen cluster ions,[2,3] hydrated hydronium ions,[4,5] ammoniated ammonium ions,[6] and some mixed cluster ions.[7]

This paper reports on the partially successful attempt to obtain high resolution spectra of two hydrated hydronium ions, $H_3O^+ \cdot H_2O$ and $H_3O^+ \cdot (H_2O)_3$. The lower resolution vibrational spectra of these two species have been presented previously[4], and the reader is referred to Refs. 4 and 5 for a thorough discussion of background information and other details.

Very little high resolution spectroscopy has been done to date on floppy ions. Two noteworthy exceptions are $ArH_3^+$ and $C_2H_3^+$. Bogey et al.[8,9] reported on the high resolution millimeter and submillimeter wave spectra of $ArH_3^+$, $ArHD_2^+$, $ArH_2D^+$ and $ArD_3^+$. They conclude that these isotopomers are planar with the argon lying near the apex of the $H_3^+$ (or substituted moiety). The Ar-$H_3^+$ centroid distance was found to be 2.38 Å with an estimated binding energy of 28 kJ/mole (6.6 kcal/mole). Because the argon is held so weakly, internal rotation of

the $H_3^+$ in the plane is expected to occur. In fact, Bogey et al. observed tunneling splittings and used these to obtain barrier heights for the internal rotation of $H_3^+$ and $D_3^+$.

More recently, Crofton et al.[10] reported on an intensive study of $C_2H_3^+$. Protonated acetylene has two structures lying close in energy: a structure with the $H^+$ bridged over both carbons and a structure with the $H^+$ attached to one carbon. Their spectrum is assigned to the lower energy bridged structure. The absorption lines are split, however, due to tunneling of the protons between the three sites in the bridged structure. A simple theoretical model for this problem is to treat the CC frame as rigid with the three protons arranged in a rotating equilateral triangle around the CC core.[11] Based on this simple model and the observed spectral splittings, an estimate of the magnitude of the barrier height was obtained.[10]

More effort has been devoted to studying the high resolution spectroscopy of floppy neutral species. Two of these, the water dimer $(H_2O)_2$, and hydrazine ($N_2H_4$), are of special interest here because of various similarities to $H_5O_2^+$. In discussing these similarities we make three assumptions: (i) the $H^+$ of $H_5O_2^+$ is located symmetrically between the two water molecules (forming a structure schematically represented by $H_2O{\cdot}H^+{\cdot}OH_2$ rather than by $H_2O{\cdot}H_3O^+$), such that the two water molecules are related to each other by a point group symmetry operation, (ii) replacement of the central proton in $H_5O_2^+$ by one of the four exterior protons is not a feasible tunneling motion, and (iii) the two water molecules in $H_5O_2^+$ are neither exactly cis nor exactly

trans to each other, so that the point group of the equilibrium configuration is $C_2$.

The water dimer[12-28] is of interest because its monomer units and its permutation-inversion group $G_{16}$ are the same as those found in $H_5O_2^+$. On the other hand, the $C_s$ point group of its equilibrium geometry is different from the $C_2$ point group of $H_5O_2^+$. Nevertheless, the previously stated facts allow us to conclude that statistical weights for the various overall $G_{16}$ symmetry species in $H_5O_2^+$ are exactly twice those for the same species in the water dimer.

Hydrazine, which was studied extensively in the microwave and far-infrared regions[29-34], is of interest because both its permutation-inversion group and the point group of its equilibrium configuration are the same as those for $H_5O_2^+$. Therefore the theoretical treatment of the tunneling problem in $H_5O_2^+$ is formally similar to that in $N_2H_4$, and the tunneling splitting expressions developed for hydrazine[31-34] (involving five purely vibrational tunneling splitting parameters) can be used without change to calculate tunneling splittings in $H_5O_2^+$.

Remington and Schaefer[35] have calculated structures, energies and vibrational frequencies for $H_3O^+ \cdot (H_2O)_n$ species with n = 1,2,3 at the SCF level using a double zeta plus polarization (DZP) basis set, and have carried out higher level CISD calculations (configuration interaction with single and double excitations) with a DZP basis set for $H_5O_2^+$. These unpublished results are summarized in some detail in Ref. 4. We shall make further use of the results of Remington and Schaefer in our discussion of intensity ratios between parallel and

perpendicular transitions, and of Coriolis coupling constants.

## Experimental Details

The experimental apparatus has been described elsewhere[4,36], and will be only briefly outlined below. Modifications in the laser scheme and data analysis necessary in these high resolution studies are explained more fully.

The cluster ions are produced in a corona discharge ion source using 26.7 kPa (200 Torr) of $H_2$ and trace quantities of $H_2O$. Following supersonic expansion and skimming, the ion beam is focussed, mass selected, and trapped in an octopole ion trap. After spectroscopic interrogation using the laser scheme described below, the trapped ions are released and fragment ions are counted using standard ion counting methods.

The laser scheme used was a two-color approach as described previously[4]. The tunable IR laser was a Burleigh cw F-center laser (FCL) as before, but now with the intracavity etalon inserted into the evacuated tuning arm chamber, giving an effective linewidth of $3 \times 10^{-5}$ $cm^{-1}$. The FCL is frequency scanned by simultaneously ramping the voltage applied to the etalon and turning a grating causing the laser to hop cavity modes which are spaced by 0.0095 $cm^{-1}$. Because we expected the Doppler width of the ions moving back and forth in the trap to be on the order of, or slightly larger than, the cavity mode spacing, we chose the mode-hopping approach over scanning the cavity length. The frequency of the FCL is scanned near the center of the band assigned to the antisymmetric O-H stretch of the $H_2O$ moieties,

i.e., near 3700 $cm^{-1}$ for $H_5O_2^+$ and 3730 $cm^{-1}$ for $H_9O_4^+$.

The second laser used was an MPB Technologies Inc. cw $CO_2$ laser. This laser is used to dissociate preferentially the vibrationally excited $H_5O_2^+$ or $H_9O_4^+$ ion through a multiphoton process. For $H_5O_2^+$, the R(24) line of the $00^01$-$02^00$ transition was used with 8 W out of the laser. The trapping time was 100 ms. In the case of $H_9O_4^+$, the $CO_2$ laser was run on R(20) of the $00^01$-$10^00$ transition, and the intensity was attenuated to 1.5 W using a gas cell containing ethylene. The trapping time used was 57.5 ms. The FCL and $CO_2$ lasers were run simultaneously into the trap in the case of $H_5O_2^+$, and were resolved temporally with a chopper for $H_9O_4^+$.

Co-adding Successive Scans and Doppler Deconvolution

As mentioned above, the F-center laser is scanned by using the computer to simultaneously ramp the voltage applied to the intra-cavity etalon and turn the grating at a rate to maintain single-mode operation. Early on, it was discovered that the mode hops did not occur reproducibly, which greatly complicated co-adding successive spectral scans. Most of the data scans were taken over slightly less than 0.5 $cm^{-1}$ in 160 channels. Since the mode hop size is 0.0095 $cm^{-1}$ the F-center laser mode hops about 50 times during these 160 channels, i.e., it hops every 3-4 channels. Using an oscilloscope to monitor these mode hops during data acquisition showed that usually the mode hops occurred every 3-4 channels, but occasionally occurred after 2 or 5 channels. In successive scans these mode hops did not occur at the same channel. Two procedures were used to compensate for this.

Data in the $^{R}R_{0}$ region were taken first. During each data scan, data acquisition was interrupted about ten times in order to measure the F-center laser frequency. The frequencies of all the intervening channels were then obtained by interpolating between these ten reference channels. In order to improve the signal-to-noise ratio, generally three data scans were taken over each frequency range with some overlap in frequency between adjacent scans. These three data sets were then plotted out and signal heights were manually measured after subtracting the background. Because of the high laser power needed to dissociate the vibrationally excited $H_5O_2^+$, some dissociation of ground state $H_5O_2^+$ also occurred. This background, of course, is independent of the F-center frequency and could be reliably subtracted assuming the $CO_2$ power and $H_5O_2^+$ ion counts remained constant. Fortunately, these assumptions seemed to be valid. The background level was generally 2/3 of the total signal. After subtracting from this baseline, the signal heights were then measured. A compilation of relative signal intensities was tabulated from 3689.0 to 3694.7 $cm^{-1}$. This raw data was then separated into groups of about 3-4 channels where the mode hops seemed to occur. The signal intensities within a given scan were then averaged over these 3-4 channels and the interpolated frequencies were also averaged. After doing this for all three independent data scans, the three data scans were then averaged both in the value of the frequencies and in the relative signal intensities. A small portion of the spectrum obtained in this way is shown in Fig. 1.

This complex and time-consuming data analysis procedure was simplified somewhat by modifying the data acquisition procedure for the $^{R}R_{1}$ branch. The mode-hopping of the F-center laser was continuously monitored on the oscilloscope and noted. Again data acquisition was interrupted several times during a data scan. Now, however, a different interpolated frequency value is obtained for groups of channels within which no mode hop occurred, rather than for every channel. The size of the mode hops varied between 0.0090 and 0.0100 $cm^{-1}$; only near the end of some data scans did the mode hop size vary markedly from 0.0095 $cm^{-1}$. This was due either to the grating being turned too quickly or too slowly with respect to the ramp on the etalon, or to the voltage ramp applied to the etalon flattening out and needing to be reset. Again three independent data scans were generally obtained for each frequency range with some overlap in frequency between adjacent groups of three scans. The spectra were plotted and signal heights measured as described in the preceding paragraph. Frequencies from 3702.0 to 3706.5 $cm^{-1}$ with relative signal intensities were then tabulated and averaged over the three scans.

During subsequent analysis using the data obtained above, a reconsideration of our expected Doppler splitting was necessary. The average energy of the ions moving back and forth in the octopole ion trap is less than 0.5 eV. Using an average energy of 0.3 eV, the Doppler shift for $H_5O_2^+$ is 0.015 $cm^{-1}$. This indicates that we should expect partial resolution of the Doppler splitting, and each spectral feature should become a doublet split by about 0.03 $cm^{-1}$. Such Doppler

splittings can clearly be seen for a number of lines in Fig. 1. Consequently, another step in an already complicated data analysis procedure was necessary; data like those in Fig. 1 were further deconvoluted taking into account this partial resolution of the Doppler splitting.

## Low Resolution Spectral Results

The spectrum of $H_5O_2^+$ taken at 0.5 $cm^{-1}$ resolution is shown in Fig. 2. This spectrum was discussed previously[4] from a vibrational point of view, so we add here only comments helpful for a discussion of the vibration-rotation spectrum. To avoid notational confusion we use upper case A,B,C to indicate rotational constants of the molecule and directions along the principal axes of inertia. We use lower case letters a,b and $a_1$,$a_2$,e to indicate symmetry species for vibrational modes in the point groups $C_2$ (for $H_5O_2^+$) and $C_{3v}$ (for $H_9O_4^+$). Furthermore, for $H_5O_2^+$ the phrases parallel band and perpendicular band have their traditional near-symmetric top meaning[37], i.e., they indicate bands with a transition dipole moment parallel or perpendicular to the near symmetric top axis, obeying rotational selection rules of $\Delta K = 0$ or $\pm 1$, respectively. (They thus do not indicate bands with a transition moment parallel or perpendicular to the $C_2$ point group symmetry axis).

$H_5O_2^+$ is a very near symmetric top, with rotational constants from the *ab initio* $C_2$ structure[35] of A = 6.120, B = 0.2936 ($C_2$ axis), and C = 0.2923 $cm^{-1}$, and an asymmetry parameter[38] $b = -1.1 \times 10^{-4}$.

Vibrational transitions from the ground state to fundamentals of a symmetry species in $C_2$ give rise to B-type perpendicular bands with selection rules $\Delta K = \pm 1$. Vibrational transitions to fundamentals of b symmetry species in $C_2$ give rise to A/C hybrid bands with selection rules $\Delta K = 0$ and $\pm 1$.

At lower frequencies we expect[35] to find the out-of-phase and in-phase combinations of the symmetric O-H stretch of each $H_2O$ unit. The out-of-phase mode is predicted[35] to lie 14 $cm^{-1}$ below the in-phase mode, and to be nearly 30 times as strong. The strong out-of-phase mode is of b symmetry species in the $C_2$ point group of the ion, and is thus an A/C hybrid band. The compact and featureless appearance of this band in Fig. 2 suggests strongly, however, that its A-type parallel component is significantly stronger than its C-type perpendicular component, in good agreement with the *ab initio* calculations, which predict a parallel to perpendicular intensity ratio $|\mu_A/\mu_C|^2$ of 6.4[35]. The in-phase mode is of a symmetry species, and would therefore appear as a purely perpendicular B-type transition, if it were strong enough to be seen.

At higher frequencies we expect[35] a nearly degenerate pair of modes formed from the antisymmetric O-H stretch of each water monomer. Here the designations in-phase and out-of-phase are ambiguous without further qualification, and it is better to speak of the a mode and the b mode. Again, the a mode is a purely perpendicular B-type band by symmetry. The b mode is an A/C hydrid band, but the fact that it is formed from a linear combination of the antisymmetric OH stretches of

the monomers (which are polarized along the H-H direction in water), together with the fact that the H-H direction in each monomer is expected to be nearly perpendicular to the $O\text{-}H^{+}\text{-}O$ near-symmetric top axis, suggests that the perpendicular component of this b mode will be much stronger than its parallel component. These qualitative arguments are in good agreement with the ab initio calculations, which predict a perpendicular to parallel intensity ratio of 119[35] for this band. The observed transition in Fig. 2, with its widely spaced Q-branch structure, looks like a perpendicular band. Indeed, the spacing between the Q branches[37] gives $2(A'-B') = 11.6\ cm^{-1}$, in remarkably good agreement with the ab initio estimate of $11.65\ cm^{-1}$. The fact that the higher frequency band in Fig. 2 looks like one perpendicular band requires Q branches from the two OH antisymmetric modes to be almost exactly coincident, if the two modes have comparable intensity. This requirement is consistent with the ab initio calculations[35], which predict two nearly degenerate modes of nearly equal intensity, as shown by the vertical dashed lines in Fig. 2.

Fermi resonance is forbidden between the nearly degenerate $\nu_1(a)$ and $\nu_2(b)$ excited antisymmetric stretch vibrational states, but Coriolis interaction between these states is in principle possible for overall angular momentum components along the inertial A or C axis of the molecule (using the ab initio structure and rotational constants). Because the A rotational constant is about $6\ cm^{-1}$, while B and C are about $0.3\ cm^{-1}$, and because Coriolis interaction energies are roughly proportional to AK, BJ or CJ, only Coriolis interaction about the A

axis will be considered. Such Coriolis interaction would cause the K spacing, i.e., the spacing of Q-branch heads at the sub-band origins, to depart from the expected[37] $c_1 + c_2K$ behavior.

The magnitude of the matrix element for off-diagonal A-axis Coriolis interaction between $\nu_1$ and $\nu_2$ is equal to $2AK\zeta_{12}^{A}$, where $\zeta_{12}^{A}$ is the appropriate Coriolis coupling constant[39]. For (hypothetical) purely stretching vibrations, Coriolis coupling constants are zero; for real molecules, such constants are typically less than 0.05. If we use the ab initio values to estimate the splittings of the Q-branch heads, we find the separation of the two antisymmetric OH stretching modes $\nu_1$-$\nu_2 \equiv \delta_{12} = 0.3$ cm$^{-1}$, and $\zeta_{12}^{(A)} = 0.0015$. These values yield energy separations between K subband origins for the two vibrations given by[39] $[\delta_{12}^2 + 16A^2(\zeta_{12}^{A})^2K^2]^{1/2} = [0.3^2 + (0.037K)^2]^{1/2}$. For upper-state values of $K \leq 5$, corresponding to the sharp Q-branches in Fig. 2, this quantity is effectively a constant, equal to 0.33 cm$^{-1}$ within 10%, and the Q-branch-head splittings induced by Coriolis interaction are thus predicted to be too small to be seen at low K and low resolution.

The spectrum of $H_9O_4^+$ taken at 0.5 cm$^{-1}$ resolution[4] is shown in Fig. 3. Ab initio calculations at the SCF level with a DZP basis set[35] lead to a $C_{3v}$ equilibrium geometry, so that $H_9O_4^+$ is rigorously an oblate symmetric top, with rotational constants from the calculated geometry[35] of A = B = 0.0876 and C = 0.0453 cm$^{-1}$. The three symmetric stretches of the $H_2O$ groups give rise to an $a_1$ vibration (in-phase combination, parallel band) and an $e$ vibration (not in-phase, perpendicular band) for the $C_{3v}$ geometry. Similarly, the three

antisymmetric stretches of the $H_2O$ units also give rise to an $\underline{a}_1$ and an $\underline{e}$ vibration. According to the intensity predictions of Remington and Schaefer[4,35], essentially all the intensity in the lower-frequency, symmetric OH stretching region is in the $\underline{e}$ perpendicular band transition. For the antisymmetric stretching region, the opposite is true, with 99% of the intensity in the $\underline{a}_1$ parallel band transition. Unfortunately, for oblate tops, it is not easy to distinguish parallel bands from perpendicular bands at low resolution, and no further comments seem appropriate for Fig. 3.

## High Resolution $H_5O_2^+$ Spectral Results

For $H_5O_2^+$, high resolution spectra were only recorded in the antisymmetric stretching region near 3700 $cm^{-1}$. Because the rather limited data set obtained[5] has not permitted an unambiguous spectral analysis, we will first consider theoretical expectations for the high resolution spectrum, and then compare these expectations with the experimental observations.

The high resolution spectrum of the antisymmetric stretching region showed many more peaks than a single vibration-rotation band of a rigid molecule allows. In addition to the presence of the two nearly degenerate vibrational bands of comparable intensity, several other factors must be considered as explanations for the extra peaks.

First is the possibility of hot bands. The corona discharge ion source is expected to have vibrational populations for the high frequency vibrations (above 1500 $cm^{-1}$) similar to those found for room temperature (i.e., less than 0.1% of the v=0 population), since high-

frequency vibrational degrees of freedom are not effectively cooled in a supersonic expansion. Very low frequency modes (though none are predicted in the ab initio calculations to lie below 164 $cm^{-1}$) would be expected to be cooled almost as efficiently as the rotational degrees of freedom. Based on the low resolution $H_5O_2^+$ spectrum, we estimate a temperature of about 42 K for the K quantum number and 14 K for J, indicating that vibrational modes at 50 $cm^{-1}$ or lower (if they exist) would certainly be significantly thermally populated in the cold beam. Estimating vibrational populations for modes in the intermediate frequency range from 50 to 1500 $cm^{-1}$ is difficult. For the worst case scenario of a 160 $cm^{-1}$ vibration with no cooling in the jet, a population ratio for (v=1)/(v=0) of 0.45 is calculated. Cooling to 42 K, however, reduces this ratio to 0.003. We conclude that hot bands, while still possible as the source of some of the additional lines observed, do not seem the most likely explanation for these lines.

A second possibility to be considered is combination bands between, for example, the symmetric OH stretches, which we observe about 100 $cm^{-1}$ below the antisymmetric stretches in the low resolution scans, and an appropriate van der Waals mode near 100 $cm^{-1}$, which would move the combination band up into the antisymmetric stretching region, or between the first overtone of the HOH bend and a van der Waals mode of appropriate frequency. Such combination and/or overtone bands could appear more strongly than expected because of intensity borrowing from one of the nearby strong antisymmetric stretching bands, particularly because van der Waals binding can change significantly upon vibrational

excitation of functional groups adjacent to the van der Waals bond. Nevertheless, we still would expect the intensity of a combination band to be noticably less than that of the fundamental from which it borrowed its intensity, so that combination bands also do not provide a good explanation for the more intense additional peaks.

Tunneling Motions

As a third possibility, the complication in the infrared spectrum could be due to splittings caused by tunneling through the low barriers found in floppy nonrigid molecules. Discussion of such splittings is greatly facilitated by the use of permutation-inversion group theory[40]. Because of our initial assumption that exchange of the central hydrogen with any other hydrogen is not a feasible motion, the central hydrogen atom of $H_2O \cdot H^+ \cdot OH_2$ does not appear in any permutation-inversion operations, and the molecular symmetry group for $H_5O_2^+$ is thus the same as that for $H_4C_2$ (ethylene), $H_4N_2$ (hydrazine), and $H_4O_2$ (water dimer). This group consists of 16 elements and is often called $G_{16}$. Unfortunately, two slightly different notations for symmetry species labels exist for $G_{16}$. The relation between these two notations can be found in Table I of Merer and Watson's paper on ethylene[41]. We shall use here the notation originally proposed by Longuet-Higgins[42], converting tunneling splitting expressions given in the alternative notation in the hydrazine literature[31-34] to the Longuet-Higgins notation.

The starting point in the determination of the energy levels will be either the nondegenerate asymmetric rotor energy levels labeled by

the quantum numbers J, $K_a$ and $K_c$, or the doubly degenerate (for K > 0) symmetric top energy levels labeled by J and K. Higher order effects in the rigid molecule, such as centrifugal distortion, can shift the nondegenerate asymmetric rotor energy levels, but cannot create additional levels. Because of the presumed $C_2$ symmetry of $H_5O_2^+$, pairs of feasible elements in $G_{16}$ acting on framework 1 yield identical final frameworks. Therefore there are eight nonsuperimposable equilibrium frameworks, and a given nondegenerate level in $H_5O_2^+$ splits into at most eight levels. The species of the levels into which a given nondegenerate level actually splits can be determined by the reverse correlation table[42,43].

The size of the shift of each of these split levels from their original degenerate position is determined by the tunneling barriers from framework 1 to each of the seven other frameworks, and by the rotational quantum numbers of the level. In the present work these shifts are dealt with as follows. We first estimate, with the help of ab initio results, the size of the tunneling barriers. Then, by comparison with other molecules whose tunneling properties have been studied, one guesses appropriate tunneling splittings for use in the J and K dependent splitting formulas below. (For this initial treatment, a number of higher order terms are neglected.) After comparing the calculated splitting patterns and predicted spectrum with the experimental spectrum, the initially chosen values for the tunneling splittings are modified to try to produce an approximate match using an iterative procedure.

For convenience we number the eight frameworks as shown in Fig. 2 of Ref. 31 (to which the reader is referred at this time), and discuss below tunneling paths 1 → n using this numbering, in the order n = 3, 5, 7, 2, and 4.

Tunneling between frameworks 1 and 3 is associated with two distinct tunneling paths, namely an internal rotation of the water molecules about the O-$H^+$-O bond, passing through a trans intermediate configuration, or a similar internal rotation in the opposite sense, passing through a cis intermediate configuration. Such internal rotations lead to observable splittings in HO-OH[44-47], $H_2N$-$NH_2$[29-34], and HNCNH[48-51], for example. For the first two of these molecules, passage through the trans barrier is much easier than passage through the cis; for the third, passage through either barrier is of similar difficulty. Because the oxygens in $H_5O_2^+$ are separated by a proton, passage through the cis or trans barrier is expected to be of nearly equal difficulty for this ion. From the structures calculated by Remington and Schaefer[35], an estimate for the trans barrier height in $H_5O_2^+$ is 3 kJ/mole (0.7 kcal/mole). Table I gives internal rotation barrier heights and tunneling splittings for a few representative molecules. Since tunneling splittings also depend on the reduced mass of the motion and the distance traveled, it is difficult to make quantitative predictions for $H_5O_2^+$ from barrier height data alone. Nevertheless, Table I suggests that internal rotation tunneling splittings may be large enough to be seen in the present experiments.

Tunneling between frameworks 1 and 5 or 6 can also occur along

either of two distinct paths. One possible path is the umbrella inversion of an $H_2O$-$H^+$ unit. Although Remington and Schaefer[35] did not calculate barrier heights, they have calculated energies for several geometries of $H_5O_2^+$ resembling expected geometries at the top of various barriers. These allow an estimate of barrier heights to be made. Using the difference between their ground state $C_2$ geometry and $C_s$ geometry (see Fig. 1 of Ref. 4), we obtain an approximate barrier height of 0.8 kJ/mole (0.2 kcal/mole) for the umbrella inversion. A second possible 1 → 5 or 6 path involves a 180° rotation of one water unit about its $C_2$ axis combined with an internal rotation of both waters about the O-$H^+$-O bond (i.e., combined with the 1 → 3 motion described above). Because this is a combined motion, it probably can be neglected, and the umbrella inversion motion will be assumed to be the dominant tunneling path from framework 1 to frameworks 5 or 6. The summary of inversion barrier heights and tunneling splittings given in Table I for other molecules suggests that inversion tunneling splittings may also be large enough to be seen in the present experiments.

Tunneling between frameworks 1 and 7 or 8 corresponds to a rotation of one $H_2O$ group about its $C_2$ axis. The 1 → 4 motion for $H_2O$-HOH in Table I is an example of a similar motion. Because the water dimer is bound much less strongly than $H_5O_2^+$, caution must be exercised in extrapolating splitting magnitudes from the dimer to the ion. Nevertheless, the fact that this motion produces the largest splitting in the water dimer (see Table I), suggests that it should be considered

for $H_5O_2^+$ also.

Tunneling between frameworks 1 and 2 is again associated with two distinct tunneling paths. One path is the simultaneous ammonia-like umbrella inversion of each $H^+$-$OH_2$ unit. This combined motion is expected to be more difficult than the inversion motion of only one $H_3O^+$ unit, i.e., more difficult than the 1 → 5 motion. The other possible tunneling path for the 1 → 2 motion is a simultaneous 180° rotation of each water molecule about its $C_2$ axis. This combined motion is expected to be more difficult than a 180° rotation of only one water unit (the 1 → 7 motion). We shall not consider 1 → 2 tunneling when calculating theoretical splitting patterns.

Tunneling between frameworks 1 and 4 requires a motion equivalent to a combined 1 → 2 and 1 → 3 motion. It is expected that this will be less feasible than either of the two individual motions, and 1 → 4 tunneling will not be considered further.

A final point to mention concerns the sign of the splitting parameters used in the energy level formulas for hydrazine splittings given in the literature and below. Since the lowest splitting component of the v = 0 energy level must have no nodes, it must be of symmetry $A_1^+$ in $G_{16}$, i.e., it must be totally symmetric. This in turn requires the three largest splitting parameters (which is all we consider in this paper) to be negative.

Energy level diagrams and statistical weights

It is instructive to compute splitting patterns for three limiting cases, namely cases in which only $1 \rightarrow 3$ splittings occur, only $1 \rightarrow 5$ splittings occur, or only $1 \rightarrow 7$ splittings occur. Because our Doppler width is estimated to be 0.03 $cm^{-1}$, and because the ab initio value for B-C is 0.0013 $cm^{-1}$, we do not expect to resolve K splittings, except for very high J states. (This conclusion must be treated with caution, however, because, in addition to structural contributions from nonzero values for B-C, large-amplitude tunneling contributions to K-type doubling are also possible.) In any case, K-type doubling effects are ignored in the energy level expressions and computed splitting patterns below.

Energy level expressions for $H_5O_2^+$ are taken to be the same as those for hydrazine[31,33], with the symmetry species changed to agree with Longuet-Higgins' notation[42], and with only the largest splitting parameter ($h_{nv}$) for each of the $1 \rightarrow n = 3$, 5, and 7 motions retained. These expressions (apart from the special case of K = 0) are given by

$$
\begin{aligned}
W(A_1^+) &= \alpha_1 + \alpha_3 + 2\alpha_5 + 2\alpha_7 \\
W(B_2^-) &= \alpha_1 - \alpha_3 + 2\alpha_5 - 2\alpha_7 \\
W(B_2^+) &= \alpha_1 + \alpha_3 - 2\alpha_5 - 2\alpha_7 \\
W(A_1^-) &= \alpha_1 - \alpha_3 - 2\alpha_5 + 2\alpha_7 \\
W(B_1^-) &= \beta_1 + \beta_3 + 2\beta_5 + 2\beta_7 \\
W(A_2^+) &= \beta_1 - \beta_3 + 2\beta_5 - 2\beta_7 \\
W(A_2^-) &= \beta_1 + \beta_3 - 2\beta_5 - 2\beta_7 \\
W(B_1^+) &= \beta_1 - \beta_3 - 2\beta_5 + 2\beta_7
\end{aligned}
\qquad (1)
$$

$$W(E^+) = (\alpha_1-\alpha_3+\beta_1+\beta_3)/2 + [(\alpha_1-\alpha_3-\beta_1-\beta_3)^2/4 + 4\gamma_5^2]^{1/2}$$
$$W(E^-) = (\alpha_1+\alpha_3+\beta_1-\beta_3)/2 + [(\alpha_1+\alpha_3-\beta_1+\beta_3)^2/4 + 4\gamma_5^2]^{1/2}$$
$$W(E^+) = (\alpha_1-\alpha_3+\beta_1+\beta_3)/2 - [(\alpha_1-\alpha_3-\beta_1-\beta_3)^2/4 + 4\gamma_5^2]^{1/2}$$
$$W(E^-) = (\alpha_1+\alpha_3+\beta_1-\beta_3)/2 - [(\alpha_1+\alpha_3-\beta_1+\beta_3)^2/4 + 4\gamma_5^2]^{1/2} ,$$

where the parameters $\alpha,\beta,\gamma$ represent tunneling matrix elements[31]

$$\alpha_n = \langle 1A|H|nA\rangle$$
$$\beta_n = \langle 1B|H|nB\rangle \qquad (2)$$
$$\gamma_n = \langle 1A|H|nB\rangle$$

between frameworks 1 and n, and between overall wavefunctions of symmetry species A or B in the $C_2$ point group of the rigid molecule equilibrium configuration. Keeping only the largest contributions to these parameters, we write[31]

$$\alpha_3 = \beta_3 = h_{3v}{}^t + (-1)^K h_{3v}{}^c$$
$$\alpha_5 = \beta_5 = (i)^K h_{5v} \qquad \text{for K even}$$
$$\alpha_5 = \beta_5 = 0 \qquad \text{for K odd}$$
$$\gamma_5 = 0 \qquad \text{for K even} \qquad (3)$$
$$\gamma_5 = (i)^{K-1} h_{5v} \qquad \text{for K odd}$$
$$\alpha_7 = \beta_7 = (i)^K h_{7v} \qquad \text{for K even}$$
$$\alpha_7 = \beta_7 = 0 \qquad \text{for K odd} .$$

Fig. 4 illustrates splitting patterns calculated from these expressions when only $1 \rightarrow 3$ splittings occur (i.e., when only $h_{3v} \neq 0$), and when trans tunneling is slightly faster than cis tunneling ($h_{3v}{}^t <$

$h_{3v}^{c} < 0$). Each K level splits into two, with a clear staggering in splitting magnitude, depending on whether K is even or odd. Fig. 5 illustrates patterns when only $1 \rightarrow 5$ splittings occur. Each K level splits into three equally spaced components; the magnitude of the splitting does not vary with K. Fig. 6 illustrates patterns when only $1 \rightarrow 7$ splittings occur. Even K levels are split into three equally spaced components; odd K levels are not split at all. Patterns when all three tunneling motions contribute to the splitting can also be calculated from Eqs. (1-3).

Overall selection rules for allowed transitions are $\Gamma^{\pm} \leftrightarrow \Gamma^{\mp}$, where $\Gamma$ represents $A_1$, $A_2$, $B_1$, $B_2$ or E. To calculate transition frequencies and thus obtain the spectral patterns shown at the bottom of Figs. 4, 5 and 6, two more questions were considered.

The first question involves the possible change in sign of the splitting parameters upon vibrational excitation. Using a somewhat crude procedure from the hydrazine literature[34] we find that the ratios $h_{3v}^{t'}/h_{3v}^{t''}$ and $h_{3v}^{c'}/h_{3v}^{c''}$ of the trans and cis $1 \rightarrow 3$ tunneling splittings in the excited (') and ground (") states are both negative ($h'' < 0$, $h' > 0$) when the a component (symmetry species in the $C_2$ point group) of the antisymmetric OH stretching vibration is excited, but are both positive ($h'' < 0$, $h' < 0$) when the b component is excited. For the purposes of Fig. 4, it was assumed that the a component was excited. Unfortunately, this crude procedure gives a ratio of zero for $h_{nv}'/h_{nv}''$ when $n = 5$ or 7. Such a result cannot predict the sign change of $h_{5v}$ and $h_{7v}$ upon OH antisymmetric stretching excitation, but

may be an indication that h' in the excited state is significantly smaller than h'' in the ground state (as drawn in Figs. 5 and 6). This phenomenon has already been observed in a number of other molecules and is thought to be related to the difficulty of transferring vibrational excitation from one side of the molecule to the other during the tunneling motion[63-65]. Spectral line patterns calculated using the above considerations (but without other intensity factors) are shown at the bottom of Figs. 4-6.

The second question involves the fact that there are two $E^+$ and two $E^-$ states, and transitions from a given $E^+$ state will in general take place to both $E^-$ states. Table VI of Ref. (31) and Table I of Ref. (32) can be used to apportion intensity between these two transitions, once the spectroscopic constants and tunneling parameters describing the upper and lower states of the transition are known. The $E^{\pm} \leftrightarrow E^{\mp}$ transitions shown in Figs. 4-6 are correct when asymmetric-rotor K-type doubling splittings are neglected (B-C = 0).

Comparison with the observed spectrum

The two high resolution scans obtained in this work are shown in Figs. 7 and 8, respectively. Fig. 7 contains part of the $^RQ_0$ branch and its associated $^RR$ branch. Fig. 8 contains part of the $^RQ_1$ branch and its associated $^RR$ branch. The clumps of lines in Fig. 8 are particularly reminiscent of a near-symmetric-top rigid-rotor subband, with its Q-branch head at the subband origin, and the associated R-branch lines going off to higher frequency with a spacing of 2B ≈ 0.5

$cm^{-1}$. The gaps in both spectra arise from water vapor absorption (in spite of nitrogen purging) of radiation from the interrogation laser.

It proved rather straightforward, by examining higher dispersion spectra similar to that shown in Fig. 1 and deconvoluting for Doppler splitting, to group essentially all of the observed R-branch peaks into series with adjacent line separations near 0.51 $cm^{-1}$. This value is slightly smaller than the (B+C) value of 0.59 $cm^{-1}$ calculated from the ab initio equilibrium structure, and is consistent with a decrease from $B_e$ to $B_o$ caused by zero-point motion in the Morse-oscillator-like potential well of the $O\text{-}H^{+}\text{-}O$ van der Waals stretch. Approximately 12 such series of lines (some less certain than others) were found for both the $^{R}R_0$ and $^{R}R_1$ branch. Tables II and III show the deconvoluted peak positions arranged according to these series. (Absolute frequency measurements are expected to be good to 0.01 $cm^{-1}$ or so, and were taken from the wave meter supplied with the Burleigh FCL.) In spite of the rather poor signal-to-noise ratio of the present data, the fact that almost all lines could be assigned to one of these series suggests strongly that the series are real branches.

The theoretical approach and assumptions adopted earlier will only give six branches after all degeneracies have been lifted. We believe that twelve branches arise because both of the predicted OH stretching vibrations are being observed, contributing six branches each. Other plausible explanations for the "extra" branches are: (i) Hot bands or combination bands are being observed.* (ii) All lines in branches not involving K = 0 levels are split into K-type doublets by large

tunneling contributions to asymmetric rotor effects. (This explanation seems improbable, since such splittings would have a strong J and K dependence, and Tables II and III indicate that the separation between branches is essentially constant with J.) (iii) The proton may not be symmetrically located between the two water molecules, and tunneling of this proton between the two resultant equivalent minima may split all levels into doublets.

The next step, clearly, is to reconcile the observed branches with a calculated spectral splitting pattern, which leads immediately to the question of which tunneling splitting dominates. Qualitatively speaking, the $1 \rightarrow 3$ spectral splitting pattern at the bottom of Fig. 4 consists of only two strong lines of equal intensity. The $1 \rightarrow 5$ splitting pattern in Fig. 5 consists of four lines with a symmetrical, but different, intensity distribution for the $K = 1 \leftarrow 0$ and $K = 2 \leftarrow 1$ transitions. The fact that nondegenerate levels are on the outside of the $1 \rightarrow 5$ level splitting pattern for even K and on the inside for odd K, combined with the presumption that the splitting in the vibrational excited state is smaller than in the ground state, leads to the two higher intensity lines being on the outside for $K = 1 \leftarrow 0$ and on the inside for $K = 2 \leftarrow 1$. The $1 \rightarrow 7$ spectral splitting pattern in Fig. 6 consists of three lines of very different intensities. It is the only splitting pattern of those under discussion with an unsymmetrical intensity distribution (which arises because the highest statistical weight lines (with intensity 12) are not split, and add together to give a line of intensity 24). In the $1 \rightarrow 7$ case, as in the $1 \rightarrow 5$ case,

we expect the level splitting in the vibrationally excited state to be smaller than in the ground state, which leads to a smaller spectral splitting in the K = 2 ← 1 transition than in the K = 1 ← 0 transition.

An attempt was made to derive an "experimental splitting pattern" to compare with these theoretical patterns by considering only the most intense member of each branch (denoted by an asterisk in Tables II and III). Finding the most intense member was relatively easy for only a few of the branches, such as branch A and B near 3703 $cm^{-1}$ in Table III. For the majority of branches, it was only possible to guess at which member was the most intense, due to the poor signal to noise. A complicating factor in choosing the most intense line is the fact that an R-branch series with K = 0 in either the upper or lower state of the transition should show some intensity alternation (or even missing lines) according to the theory used here. There seems to be some indication of intensity alternation (see, for example, branches A, C and D near 3693 $cm^{-1}$ in Table II), but the present intensity data is not reliable enough to state this with any certainty.

Since the splitting pattern formed by the asterisked lines in Table II is not obviously symmetrical, an initial trial spectral splitting pattern was calculated with 1 → 7 as the dominant motion and 1 → 3 as the secondary motion. This pattern is shown in Fig. 9, where one might try to match the asterisked lines from branches A,B and J,K in Table II with the four strongest lines in the K = 1 ← 0 pattern shown for one O-H stretching vibration at the bottom of Fig. 9. The asterisked lines from branches D,E could then arise from the other

antisymmetric O-H stretching vibration, and would correspond to the two strongest lines in its $K = 1 \leftarrow 0$ pattern. We examined a number of initial identifications of this kind, but were unable to carry any of them forward and find a set of parameters which gave a calculated spectrum clearly resembling the observed one.

At this point, because the desired quantitative comparison of theoretical and experimental splitting patterns could not be achieved, we turned to a qualitative examination of the high-resolution Q branch scans, hoping to use the total "width" of a given unresolved Q-branch clump as an upper bound for the magnitude of the tunneling splittings, or to determine if the splitting barely visible in the medium resolution $^{R}Q_1$ branch scan shown in Fig. 2 is real. Unfortunately, gaps in the high resolution spectra shown in Figs. 7 and 8 caused by water vapor absorption prevent us from obtaining even this qualitative information on the tunneling splittings.

## High Resolution $H_9O_4^+$ Spectral Results

The high resolution $H_9O_4^+$ spectrum is shown in Fig. 10. It can be seen that spectral density and resolution are such that individual lines are not resolved. However, some comments seem in order.

As in the case of $H_5O_2^+$, possible sources of complication in the spectrum include hot bands, overtone or combination bands, and tunneling splittings. Many of the arguments presented earlier for $H_5O_2^+$ carry over to $H_9O_4^+$ and we discuss here only some possible sources of tunneling splittings.

If the antisymmetric stretching vibration centered near 3730 $cm^{-1}$

is indeed due to a parallel band transition as predicted by Remington and Schaefer[35], the features in the P and R branches should be spaced at 2B intervals. The incompletely resolved structure shown in Fig. 10 below 3730 $cm^{-1}$ and above 3732 $cm^{-1}$ is spaced by 0.17 $cm^{-1}$, which agrees well with the value of 0.175 $cm^{-1}$ from ab initio structure calculations.

An interesting portion of the spectrum lies between 3730 and 3732 $cm^{-1}$, where there appear to be two pairs of strong features. The pairs are separated by 0.93 $cm^{-1}$ and the members of each pair by 0.21 $cm^{-1}$. Each of these splittings may arise from some tunneling motion. One likely source of tunneling splittings in $H_9O_4^+$ is a rotation of the end $H_2O$ groups about the water monomer $C_2$ axes. Because there are three $H_2O$ monomers, this motion could potentially give non-identical splittings from in-phase and out-of-phase components.

Another possible tunneling motion through a low barrier is the inversion motion of the central $H_3O^+$ moiety. By using the higher energy $D_{3h}$ structure calculated by Remington and Schaefer[35] to represent the structure at the top of the inversion barrier, the barrier height can be estimated to be about 2.3 kJ/mole (0.55 kcal/mol). This barrier height and geometrical information from the ab initio calculation were used to construct a rough double well potential, from which tunneling splittings were obtained using a program written by Gruebele[66]. A critical unknown parameter in this calculation is the reduced mass of the inversion motion. If the motion consists solely of the central oxygen moving up and down, a reduced

mass of 12.5 is obtained. Because the actual motion is more complicated and involves more than the central oxygen, the effective reduced mass will be somewhat larger. Using a value of 18 leads to a spectral splitting of about 3 $cm^{-1}$, making it a candidate for explanation of the experimentally observed splittings. From the data we obtained, no conclusions can be made as to the relative magnitudes of these particular tunneling splittings or even if they are the ones responsible for the complexity in the observed spectrum.

## Discussion

Further progress in analysis of the spectrum of $H_5O_2^+$ requires a set of careful scans which improve on four major areas. The first area is elimination of the gaps in the high resolution spectrum due to water vapor absorption, which could be accomplished using either a cw laser system with more efficient purging or a pulsed laser system. Even a scan taken with medium resolution would be extremely useful to see if additional Q branch lines lie in the two gaps. The second area needing improvement is the signal-to-noise. Reliable intensity information would allow a definitive K assignment because of the intensity alternation in subbands involving K = 0. The third improvement would be to use a continuous rather than a mode-hopping laser scanning procedure. This would greatly improve the precision of line-position measurements and knowledge of lineshapes. Finally, further progress would be easier if Doppler splittings, which degrade the resolution and further complicate an already congested spectrum, could be eliminated.

A very careful ab initio study of barrier heights for the more plausible tunneling paths would be helpful, but even reliable relative values for such small barriers may tax present computational methods, since, for example, Lee and Dyke[67] found in their recent ab initio study of complexes of the form $H(H_2O)_n^+$ for n = 1 to 5, that the dihedral angle in the $C_2$ minimum-energy form of $H(H_2O)_2^+$ is both basis-set and method dependent. These authors conclude that "larger basis sets are required to exhaust the basis set effects on these computed parameters."

Before concluding, it should be stressed that we have used a formalism designed for large amplitude motions in hydrazine to describe $H_5O_2^+$, even though there is as yet only intuition, and no experimental evidence, suggesting this to be a reasonable approach. The weakest point in this approach is probably the necessity that the central proton be symmetrically located between the two water molecules. An unsymmetrical equilibrium position for the central proton would generate twice as many frameworks for the ion and render almost all theoretical considerations in this paper inapplicable.

## ACKNOWLEDGMENT

The authors are greatly indebted to Richard Remington and Prof. H. F. Schaefer for providing detailed printouts of the vibrational normal mode vectors, transition moments, Coriolis coupling constants, etc. obtained from their ab initio calculations. LIY acknowledges the assistance of James Myers during the data acquisition and Dr. Douglas J. Krajnovich in the data analysis. The authors would also like to thank Dr. Martin Gruebele for the use of his program to obtain a splitting magnitude for $H_9O_4^+$. This work was supported by the Director, Office of Energy Research, Office of Basic Energy Sciences, Chemical Sciences Division of the U. S. Department of Energy under Contract No. DE-AC03-76SF00098.

## References


1. J. V. Coe and R. J. Saykally, in Ion and Cluster Ion Spectroscopy and Structure, edited by J. P. Maier (Elsevier, Amsterdam, 1989), pp. 131-154.
2. M. Okumura, L. I. Yeh, and Y. T. Lee, J. Chem. Phys. **83**, 3705 (1985).
3. M. Okumura, L. I. Yeh, and Y. T. Lee, J. Chem. Phys. **88**, 79 (1988).
4. L. I. Yeh, M. Okumura, J. D. Myers, J. M. Price, and Y. T. Lee, J. Chem. Phys. **91**, 7319 (1989). Certain commercial instruments and materials are identified in this reference and the present paper in order to specify adequately the experimental procedure. In no case does such identification imply recommendation or endorsement by the National Institute of Standards and Technology, nor does it imply that the instruments or materials identified are necessarily the best available for the purpose.
5. L. I. Yeh, Ph. D. thesis, University of California, Berkeley, 1988.
6. J. M. Price, M. W. Crofton, and Y. T. Lee, J. Chem. Phys. **91**, 2749 (1989).
7. M. Okumura, L. I. Yeh, J. D. Myers, and Y. T. Lee, J. Phys. Chem. **94**, 3416 (1990).
8. M. Bogey, H. Bolvin, C. Demuynck, and J. L. Destombes, Phys. Rev. Lett. **58**, 988 (1987).
9. M. Bogey, H. Bolvin, C. Demuynck, J. L. Destombes, and B. P. Van Eijck, J. Chem. Phys. **88**, 4120 (1988).

10. M. W. Crofton, M.-F. Jagod, B. D. Rehfuss, and T. Oka, J. Chem. Phys. **91**, 5139 (1989).

11. J. T. Hougen, J. Mol. Spectrosc. **123**, 197 (1987).

12. T. R. Dyke, J. Chem. Phys. **66**, 492 (1977).

13. T. R. Dyke, K. M. Mack, and J. S. Muenter, J. Chem. Phys. **66**, 498 (1977).

14. J. A. Odutola and T. R. Dyke, J. Chem. Phys. **72**, 5062 (1980).

15. L. H. Coudert, F. J. Lovas, R. D. Suenram, and J. T. Hougen, J. Chem. Phys. **87**, 6290 (1987).

16. L. Martinache, S. Jans-Bürli, B. Vogelsanger, W. Kresa and A. Bauder, Chem. Phys. Lett. **149**, 424 (1988).

17. J. A. Odutola, T. A. Hu, D. Prinslow, S. E. O'Dell and T. R. Dyke, J. Chem. Phys. **88**, 5352 (1988).

18. T. A. Hu and T. R. Dyke, J. Chem. Phys. **91**, 7348 (1989).

19. K. L. Busarow, R. C. Cohen, G. A. Blake, K. B. Laughlin, Y. T. Lee and R. J. Saykally, J. Chem. Phys. **90**, 3937 (1989).

20. G. T. Fraser, R. D. Suenram and L. H. Coudert, J. Chem. Phys. **90**, 6077, (1989).

21. G. T. Fraser, R. D. Suenram, L. H. Coudert and R. S. Frye, J. Mol. Spectrosc. **137**, 244 (1989).

22. Z. S. Huang and R. E. Miller, J. Chem. Phys. **88**, 8008 (1988).

23. Z. S. Huang and R. E. Miller, J. Chem. Phys. **91**, 6613 (1989).

24. E. Zwart, J. J. ter Meulen, and W. L. Meerts, Chem. Phys. Lett. **166**, 500 (1990).

25. E. Zwart, J. J. ter Meulen, W. L. Meerts, and L. H. Coudert, J. Mol. Spectrosc. **147**, 27 (1991).

26. J. T. Hougen, J. Mol. Spectrosc. **114**, 395 (1985).

27. L. H. Coudert and J. T. Hougen, J. Mol. Spectrosc. **130**, 86 (1988).

28. L. H. Coudert and J. T. Hougen, J. Mol. Spectrosc. **139**, 259 (1990).

29. T. Kasuya, Sci. Papers Inst. Phys. Chem. Res. **56**, 1 (1962)

30. T. Kasuya and T. Kojima, J. Phys. Soc. Japan, **18**, 364 (1963).

31. J. T. Hougen, J. Mol. Spectrosc. **89**, 296 (1981).

32. S. Tsunekawa, T. Kojima, and J. T. Hougen, J. Mol. Spectrosc. **95**, 133 (1982).

33. N. Ohashi and J. T. Hougen, J. Mol. Spectrosc. **112**, 384 (1985).

34. N. Ohashi, W. J. Lafferty, and W. B. Olson, J. Mol. Spectrosc. **117**, 119 (1986).

35. R. Remington and H. F. Schaefer, unpublished results.

36. S. W. Bustamente, M. Okumura, D. Gerlich, H. S. Kwok, L. R. Carlson, and Y. T. Lee, J. Chem. Phys. **86**, 508 (1987).

37. G. Herzberg, Infrared and Raman Spectra of Polyatomic Molecules (Van Nostrand, New York, 1945).

38. H. C. Allen, Jr. and P. C. Cross, Molecular Vib-Rotors (Wiley, New York, 1963).

39. W. L. Smith and I. M. Mills, J. Chem. Phys. **40**, 2095 (1964).

40. P. R. Bunker, Molecular Symmetry and Spectroscopy (Academic Press, Inc., New York, 1979).

41. A. J. Merer and J. K. G. Watson, J. Mol. Spectrosc. **47**, 499 (1973).

42. H. C. Longuet-Higgins, Mol. Phys. **6**, 445 (1963).

43. J. K. G. Watson, Can. J. Phys. **43**, 1996 (1965).

44. R. L. Redington, W. B. Olson, and P. C. Cross, J. Chem. Phys. **36**, 1311 (1962).

45. R. H. Hunt, R. A. Leacock, C. W. Peters, and K. T. Hecht, J. Chem. Phys. **42**, 1931 (1965).

46. J. T. Hougen, Can. J. Phys. **62**, 1392 (1984).

47. J.-M. Flaud, C. Camy-Peyret, J. W. C. Johns and B. Carli, J. Chem. Phys. **91**, 1504 (1989).

48. M. Birk and M. Winnewisser, Chem. Phys. Lett. **123**, 386 (1986).

49. M. T. Nguyen, N. V. Riggs, L. Radom, M. Winnewisser, B. P. Winnewisser and M. Birk, Chem. Phys. **122**, 305 (1988).

50. M. Winnewisser and M. Birk, J. Chem. Soc., Faraday Trans. 2 **84**, 1341 (1988).

51. M. Birk, M. Winnewisser and E. A. Cohen, J. Mol. Spectrosc. **136**, 402 (1989).

52. N. Ohashi, J. Mol. Spectrosc. **137**, 242 (1989).

53. R. Fantoni, K. van Helvoort, W. Knippers and J. Reuss, Chem. Phys. **110**, 1 (1986).

54. W. B. Olson and D. Papousek, J. Mol. Spectrosc. **37**, 527 (1971).

55. P. R. Bunker and H. C. Longuet-Higgins, Proc. Roy. Soc. (London) **280A**, 340 (1964).

56. L. Coudert and A. Valentin, J. Mol. Spectrosc. **122**, 390 (1987).

57. V. Stern, C. Belorgeot, J. Kachmarsky and K. D. Möller, J. Mol. Spectrosc. **67**, 244 (1977).

58. N. Ohashi, K. Takagi, J. T. Hougen, W. B. Olson and W. J. Lafferty, J. Mol. Spectrosc. **132**, 242 (1988).

59. C. H. Townes and A. L. Schawlow, Microwave Spectroscopy (Dover Publications Inc, New York, 1975).

60. T. J. Sears, P. R. Bunker, P. B. Davies, S. A. Johnson and V. Spirko, J. Chem. Phys. **83**, 2676 (1985).

61. D.-J. Liu, T. Oka and T. J. Sears. J. Chem. Phys. **84**, 1312 (1986).

62. B. J. Smith, D, J. Swanton, J. A. Pople, H. F. Schaefer, III, and L. Radom, J. Chem. Phys. **92**, 1240 (1990).

63. A. S. Pine, W. J. Lafferty and B. J. Howard, J. Chem. Phys. **81**, 2939 (1984).

64. I. M. Mills, J. Phys. Chem. **88**, 532 (1984).

65. G. T. Fraser, J. Chem. Phys. **90**, 2097 (1989).

66. M. Gruebele, private communication.

67. E. P. F. Lee and J. M. Dyke, Mol. Phys. **73**, 375 (1991).

Table I

Barrier Heights and Tunneling Splittings for Selected Molecules and Large Amplitude Motions

INTERNAL ROTATION[a]

| Molecule | | Barrier Height[b] | | Splitting[c] | |
|---|---|---|---|---|---|
| HO-OH | trans | 1.1 | [47] | 11.4 | [45] |
| | cis | 7.3 | [47] | < 0.002 | [45] |
| HNCNH | trans | 5.7 | [51] | 0.0076 | [50] |
| | cis | 5.7 | [51] | 0.0091 | [50] |
| $H_2N$-$NH_2$ | trans | 3.6 | [52] | 0.0002 | [52] |
| | cis | 13.1 | [52] | - | |
| $H_2OH^+OH_2$ | trans | 0.7 | [35] | ? | |
| | cis | ? | | ? | |
| $H_3C$-$CH_3$ | | 2.9 | [53] | 0.006 | [53] |
| $H_3CCCCH_3$ | | < 0.01 | [54] | d | [54,55] |
| $H_3C$-OH | | 1.1 | [56] | 9.1 | [57] |
| $H_3C$-$NH_2$ | | 2.0 | [58] | 0.25 | [58] |

INVERSION[e]

| Molecule | Barrier[b] | | Splitting[c] | |
|---|---|---|---|---|
| $NH_3$ | 5.9 | [59] | 0.8 | [59] |
| $H_3O^+$ | 1.9 | [60] | 55.3 | [61] |
| $H_2NNH_2$ | 2.8 | [30] | 0.5 | [30] |
| $H_2OH^+OH_2$ | 0.2 | [35] | ? | |
| $H_3CNH_2$ | 6.6 | [58] | 0.2 | [58] |
| $OH_3^+(OH_2)_3$ | 0.6 | [35] | ? | |

$H_2OHOH$

| Motion[f] | Barrier[b] | | Splitting[c] | |
|---|---|---|---|---|
| 1 → 4 | 0.6 | [62] | 3.2 | [28] |
| 1 → 5,6 | 0.9 | [62] | 0.7 | [28] |
| 1 → 2 | 1.9 | [62] | 0.05 | [28] |

[a]Examples of molecules exhibiting internal rotation, grouped according to molecular structure. When internal rotation takes place about a single bond, this bond is indicated by a dash in the molecular formula.
[b]Barrier heights in kcal/mole. Numbers in square brackets are literature references.
[c]Tunneling splittings in $cm^{-1}$. Numbers in square brackets are literature references.
[d]The concept of tunneling splittings must be replaced by free rotor energy level spacings in this very low barrier case.
[e]Examples of molecules exhibiting inversion, grouped according to molecular structure.
[f]The water dimer exhibits a number of tunneling motions which are neither pure internal rotations nor pure inversions. These are labeled here simply by initial and final framework number.

Table II

Line Positions[a] and Relative Intensities[b] for Branches[c] in the $^{R}R_{0}$ Region

| A | | B | | C | | D | | E | | F | |
|---|---|---|---|---|---|---|---|---|---|---|---|
| | | | | | | 3691.663 | (6) | 3691.682 | (4) | 3691.743 | (3.5) |
| 3692.042 | (6) | 3692.074 | (4) | 3692.120 | (3.5) | 3692.156 | (2) | | | 3692.208 | (2.5) |
| *3692.532 | (9) | *3692.560 | (8) | *3692.615 | (6.5) | 3692.640 | (4) | 3692.674 | (3) | 3692.716 | (2) |
| 3693.020 | (6) | 3693.050 | (6.5) | 3693.105 | (4.5) | 3693.145 | (6) | 3693.192[d] | (3) | 3693.192[d] | (3) |
| 3693.551 | (6) | 3693.575 | (3.5) | 3693.610 | (5) | *3693.637 | (8) | *3693.668 | (6) | *3693.718 | (7) |
| 3694.053 | (1.5) | 3694.083 | (3) | 3694.127 | (4) | 3694.148 | (4) | 3694.168 | (4) | 3694.228 | (2.5) |
| 3694.578 | (4) | 3694.606 | (3) | 3694.653 | (6) | | | | | | |

| G | | H | | I | | J | | K | | L | |
|---|---|---|---|---|---|---|---|---|---|---|---|
| | | | | | | | | | | 3691.950 | (4) |
| 3692.267 | (3) | 3692.329 | (5.5) | 3692.348 | (4) | 3692.405 | (5.5) | 3692.423 | (3) | 3692.470 | (2.5) |
| 3692.764 | (2.5) | 3692.795 | (3) | 3692.846 | (5) | *3692.897 | (7) | *3692.926 | (5) | 3692.992 | (2.5) |
| 3693.281 | (4) | | | 3693.334 | (4) | 3693.360 | (5) | 3693.416 | (2) | 3693.496 | (3.5) |
| 3693.749 | (4.5) | 3693.791 | (1.5) | 3693.836 | (4.5) | 3693.874 | (5) | 3693.915 | (3.5) | 3693.995 | (3) |
| 3694.274 | (2) | | | 3694.333 | (5) | | | 3694.407 | (2) | 3694.477 | (4) |

[a]Line positions are in $cm^{-1}$.
[b]Estimated relative intensities are in parentheses. The strongest line in the intensity pattern of a given branch (when obvious) is indicated by an asterisk.
[c]The twelve branches found are labeled by the letters A through L. Line spacings within each branch correspond to B+C values near 0.5 $cm^{-1}$.
[d]This line is assigned to both branch E and branch F.

Table III

Line Positions[a] and Relative Intensities[b] for Branches[c] in the $^{R}R_{1}$ Region

| A | | B | | C | | D | | E | | F | |
|---|---|---|---|---|---|---|---|---|---|---|---|
| | | | | | | 3702.819 | (4.5) | 3702.881 | (2.5) | 3702.910 | (4.5) |
| 3703.210 | (6) | 3703.267 | (3) | 3703.300 | (5) | 3703.343 | (3.5) | 3703.370 | (3) | 3703.404 | (2.5) |
| 3703.725 | (9) | 3703.753 | (4) | 3703.811 | (4) | 3703.859 | (5) | 3703.889 | (5) | | |
| 3704.247 | (10) | 3704.275 | (4) | 3704.327 | (7) | 3704.355 | (5) | 3704.393 | (5.5) | 3704.434 | (2) |
| *3704.766 | (10) | 3704.809 | (7) | | | 3704.868 | (6) | *3704.902 | (6) | 3704.953 | (2.5) |
| 3705.293 | (10) | *3705.329 | (7) | | | 3705.377 | (4) | 3705.404 | (6) | 3705.467 | (3) |
| 3705.834 | (8) | 3705.891 | (7) | | | 3705.958 | (4) | 3705.982 | (5) | 3706.014 | (3) |
| 3706.335 | (4) | 3706.374 | (4) | | | | | 3706.442 | (3) | 3706.471 | (3) |

| G | | H | | I | | J | | K | | L | |
|---|---|---|---|---|---|---|---|---|---|---|---|
| 3702.944 | (4.5) | 3703.016 | (3.5) | 3703.050 | (3) | 3703.085 | (4) | 3703.113 | (3) | 3703.173 | (4) |
| 3703.449 | (3) | 3703.524 | (3.5) | 3703.552 | (3.5) | 3703.596 | (3.5) | 3703.620 | (3) | 3703.673 | (5) |
| 3703.972 | (3) | 3704.051 | (2) | 3704.087 | (3) | 3704.115 | (2.5) | 3704.181 | (2) | 3704.209 | (5) |
| 3704.478 | (3) | 3704.561 | (3) | 3704.609 | (4) | 3704.640 | (2.5) | 3704.689 | (2) | 3704.733 | (6) |
| 3705.002 | (4) | 3705.060 | (3) | | | 3705.155 | (2) | 3705.213 | (3) | 3705.241 | (3) |
| 3705.510 | (5) | 3705.563 | (3) | 3705.635 | (4) | 3705.696 | (4) | 3705.749 | (3) | 3705.791 | (6) |
| | | 3706.065 | (3) | 3706.149 | (2) | 3706.187 | (3) | 3706.244 | (2.5) | | |

[a]Line positions are in $cm^{-1}$.

[b]Estimated relative intensities are in parentheses. The strongest line in the intensity pattern of a given branch (when obvious) is indicated by an asterisk.

[c]The twelve branches found are labeled by the letters A through L. Line spacings within each branch correspond to B+C values near 0.5 $cm^{-1}$.

## CAPTIONS FOR FIGURES

Fig. 1

A segment of the high resolution spectrum obtained as described in the text. The uneveness of the frequency spacing of the vertical lines, which correspond to individual data points, is a consequence of the averaging procedure described in the text. Leading lines A,B,C,D above the spectrum indicate the positions of four of the branches. The closely spaced doublets in each branch represent partially resolved Doppler components; the widely spaced doublets represent the B+C separation between adjacent lines in a branch. The signal-to-noise ratio of the strongest lines is about 10.

Fig. 2

Low resolution ($\Delta\nu \approx 0.5$ cm$^{-1}$) infrared spectrum of $H_5O_2^+$ taken using the F-center laser and $CO_2$ laser. The higher frequency band, centered at 3684.4 cm$^{-1}$, is a perpendicular band and is assigned to the antisymmetric O-H stretch of an $H_2O$ moiety. The lower band, at 3608.8 cm$^{-1}$, is the symmetric O-H stretch of an $H_2O$ unit. The dashed lines correspond to the frequencies and intensities calculated in Ref. 35 for the $C_2$ structure.

Fig. 3

Low resolution ($\Delta\nu \approx 0.5$ cm$^{-1}$) infrared spectrum of $H_9O_4^+$ taken with the F-center laser and $CO_2$ laser. The antisymmetric O-H stretch of an outer $H_2O$ unit is located at 3730.4 cm$^{-1}$, and the symmetric stretch at 3644.9 cm$^{-1}$. The dashed lines correspond to the frequencies and intensities calculated in Ref. 35 for the $C_{3v}$ structure.

Fig. 4

Calculated splitting patterns for K = 0, 1 and 2 for torsion about the O-$H^+$-O axis. The arbitrary constants $h_{3v}^t$ = -0.055 $cm^{-1}$ and $h_{3v}^c$ = -0.015 $cm^{-1}$ were used for v = 0; the negatives of these values were used for v = 1. In both cases, $|h_{3v}^t| > |h_{3v}^c|$. Symmetry species labels represent the following: $\Gamma_1 = A_1^+(2) + B_2^+(12) + E^-(6)$, $\Gamma_2 = A_1^-(2) + B_2^-(12) + E^+(6)$, $\Gamma_3 = A_2^-(6) + B_1^-(0) + E^+(6)$, and $\Gamma_4 = A_2^+(6) + B_1^+(0) + E^-(6)$. The numbers in parentheses are statistical weights (5), which are just twice the corresponding values for $(H_2O)_2$ (12). The spectral splitting pattern for a given vibration-rotation transition shown at the bottom of the figure is drawn with an expanded scale compared to the splitting patterns of the levels.

Fig. 5

Calculated splitting patterns for K = 0, 1 and 2 for inversion of an $H_2O$-$H^+$ unit. The constant $h_{5v}$ is assumed to be negative for both v = 0 and v = 1, and to be larger in magnitude for v = 0. Symmetry species labels are: $\Gamma_5 = A_1^+(2) + B_2^-(12)$, $\Gamma_6 = E^+(6) + E^-(6)$, $\Gamma_7 = A_1^-(2) + B_2^+(12)$, $\Gamma_8 = A_2^+(6) + B_1^-(0)$, $\Gamma_9 = A_2^-(6) + B_1^+(0)$, $\Gamma_{10} = \Gamma_5 + \Gamma_7 + \Gamma_8 + \Gamma_9$. Numbers in parentheses are statistical weights. Spectral splitting patterns at the bottom are drawn on an expanded scale.

Fig. 6

Calculated splitting patterns for K = 0, 1 and 2 for rotation of an $H_2O$ moiety about its $C_2$ axis. The constant $h_{7v}$ is assumed to be negative for both v = 0 and v = 1, and to be larger in magnitude for v = 0. Symmetry species labels are: $\Gamma_{11} = A_1^+(2) + A_1^-(2)$, $\Gamma_{12} = E^+(6) +$

$E^-(6)$, $\Gamma_{13} = B_2^+(12) + B_2^-(12)$, $\Gamma_{14} = B_1^+(0) + B_1^-(0)$, $\Gamma_{15} = A_2^+(6) + A_2^-(6)$, $\Gamma_{16} = \Gamma_{11} + 2\Gamma_{12} + \Gamma_{13} + \Gamma_{14} + \Gamma_{15}$. Numbers in parentheses are statistical weights.

Fig. 7

High resolution scan of $H_5O_2^+$ in the region of the $^RQ_0$ branch obtained by mode hopping the F-center laser (mode separation $\sim$ 0.010 $cm^{-1}$). The resolution is Doppler limited and estimated to be 0.01 $cm^{-1}$. The 1.2 $cm^{-1}$ gap near 3691 $cm^{-1}$ is due to residual water vapor absorption not removed by the nitrogen purging. Leading lines indicate the same branches and (B+C) separations as in Fig. 1.

Fig. 8

High resolution scan of $H_5O_2^+$ in the region of the $^RQ_1$ branch under conditions as described for Fig. 7. The feature at 3702.4 $cm^{-1}$ may be the upper tunneling splitting component of the Q branch. Suggestions of the lower component can be seen in the low resolution scans at about 3701.4 $cm^{-1}$, which unfortunately lies in a region of attenuated F-center laser power in Fig. 8.

Fig. 9

Calculated splitting patterns for K = 0, 1 and 2 assuming rotation of an $H_2O$ moiety about its $C_2$ axis (the 1 → 7 motion) gives rise to the largest splitting, and torsion around the $O\text{-}H^+\text{-}O$ bond (the 1 → 3 motion) gives rise to a smaller splitting. The constant $h_{7v}$ is assumed to be negative for both v = 0 and v = 1, and to be larger in magnitude for v = 0 (see Fig. 6). The constant $h_{3v}{}^t$ is assumed to have equal and opposite values in v = 0 and 1 (see Fig. 4); the ground state value is

negative, and the magnitude is smaller than that of $h_{7v}$. Symmetry species labels are: $\Gamma_1 = A_1^+(2)$, $\Gamma_2 = A_1^-(2)$, $\Gamma_3 = \Gamma_{10} = E^-(6)$, $\Gamma_4 = \Gamma_9 = E^+(6)$, $\Gamma_5 = B_2^+(12)$, $\Gamma_6 = B_2^-(12)$, $\Gamma_7 = B_1^-(0)$, $\Gamma_8 = B_1^+(0)$, $\Gamma_{11} = A_2^-(6)$, $\Gamma_{12} = A_2^+(6)$, $\Gamma_{13} = \Gamma_1 + \Gamma_3 + \Gamma_5 + \Gamma_7 + \Gamma_9 + \Gamma_{11}$, $\Gamma_{14} = \Gamma_2 + \Gamma_4 + \Gamma_6 + \Gamma_8 + \Gamma_{10} + \Gamma_{12}$. Numbers in parentheses are statistical weights.

Fig. 10

High resolution scan of $H_9O_4^+$ obtained by exciting the antisymmetric stretch of an outer $H_2O$ moiety. The lines on either side of the central features are separated by 2B. The central features may be Q-branches which have been split by tunneling motions such as the umbrella inversion mode of the $H_3O^+$ core.

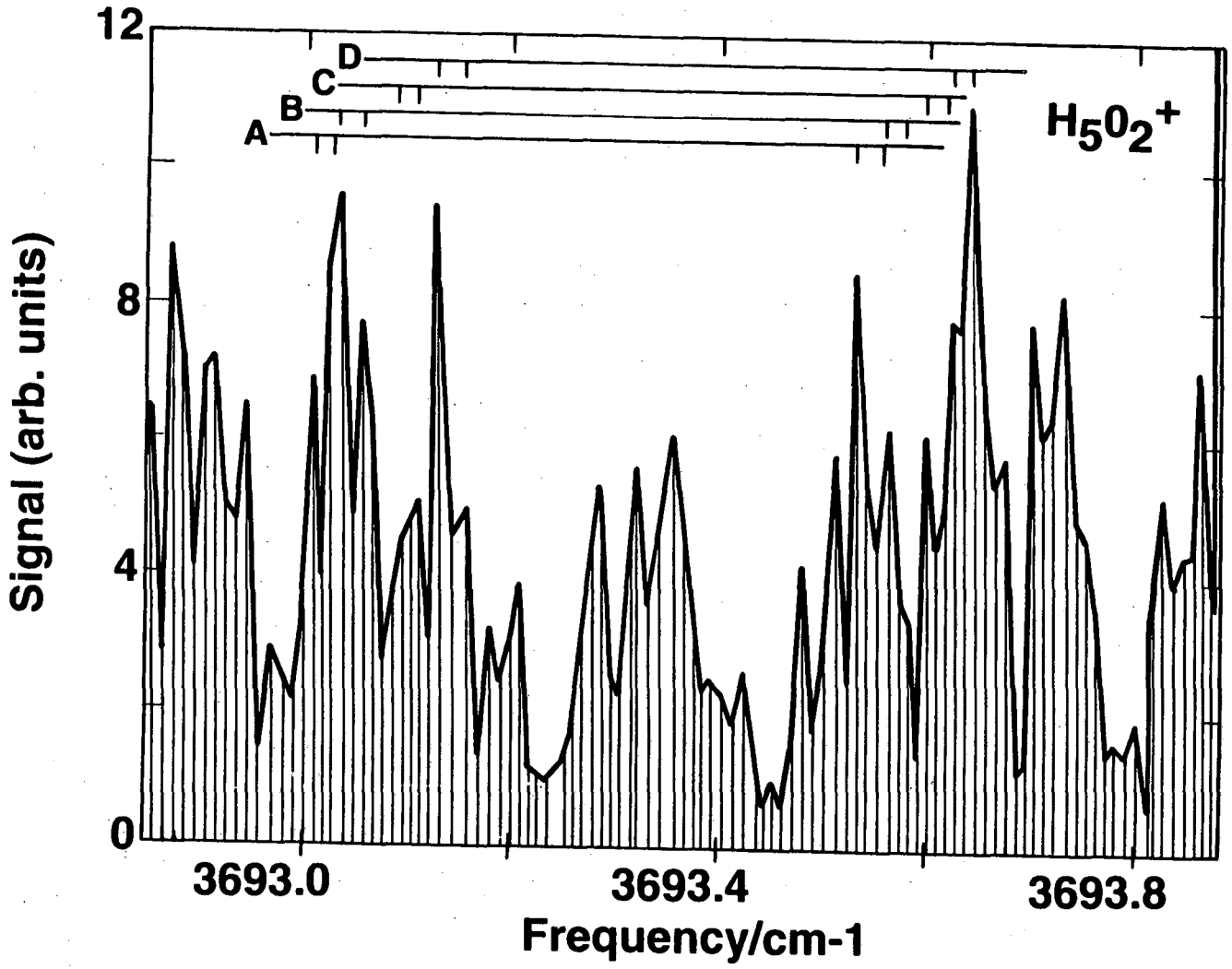
12
8
4
0
Signal (arb. units)
A
B
C
D
$H_5O_2^+$
3693.0
3693.4
3693.8
Frequency/cm-1

Fig. 1

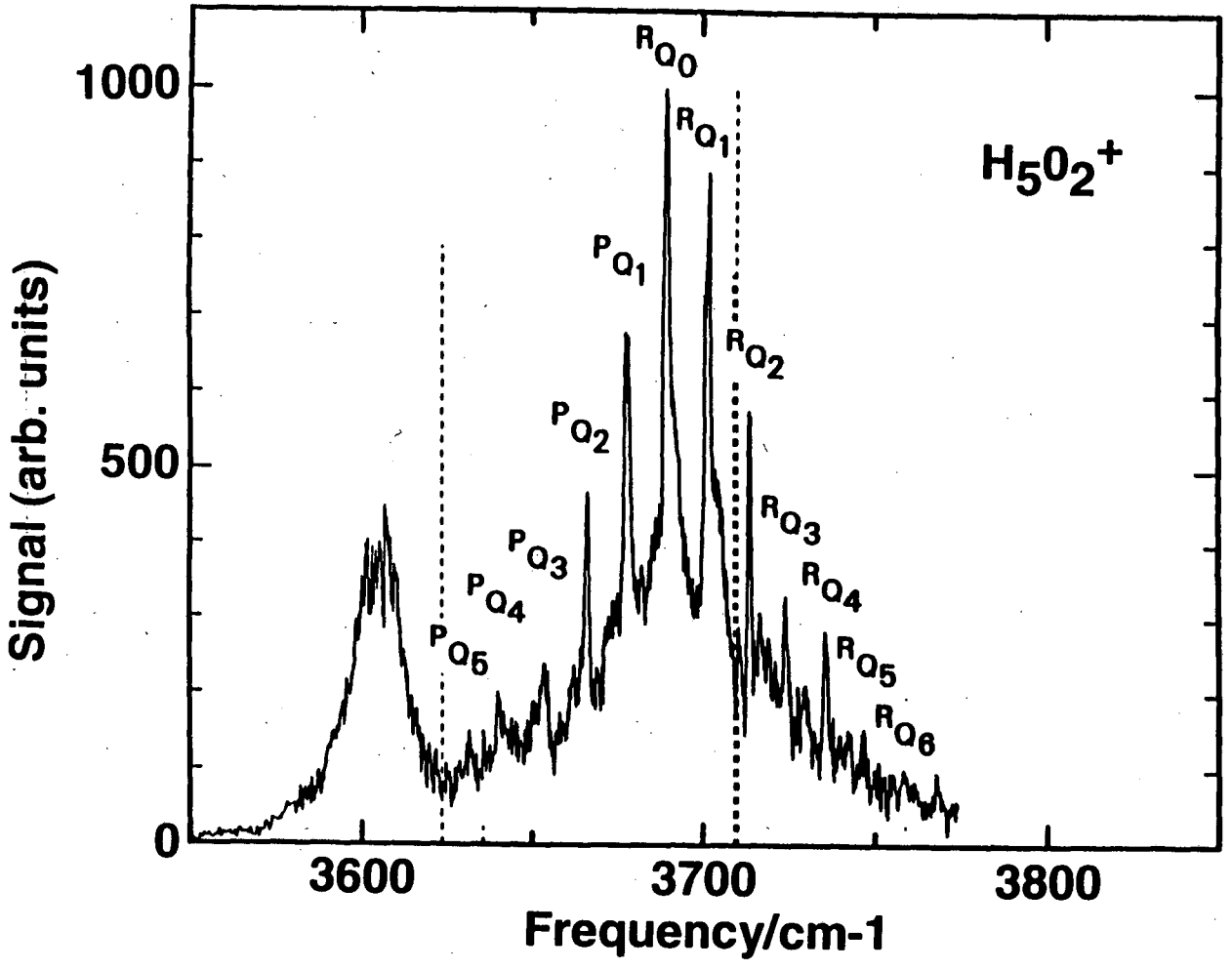
1000
500
0
Signal (arb. units)
3600
3700
3800
Frequency/cm-1
$H_5O_2^+$
$R_{Q_0}$
$R_{Q_1}$
$P_{Q_1}$
$R_{Q_2}$
$P_{Q_2}$
$R_{Q_3}$
$P_{Q_3}$
$R_{Q_4}$
$P_{Q_4}$
$R_{Q_5}$
$P_{Q_5}$
$R_{Q_6}$

Fig. 2

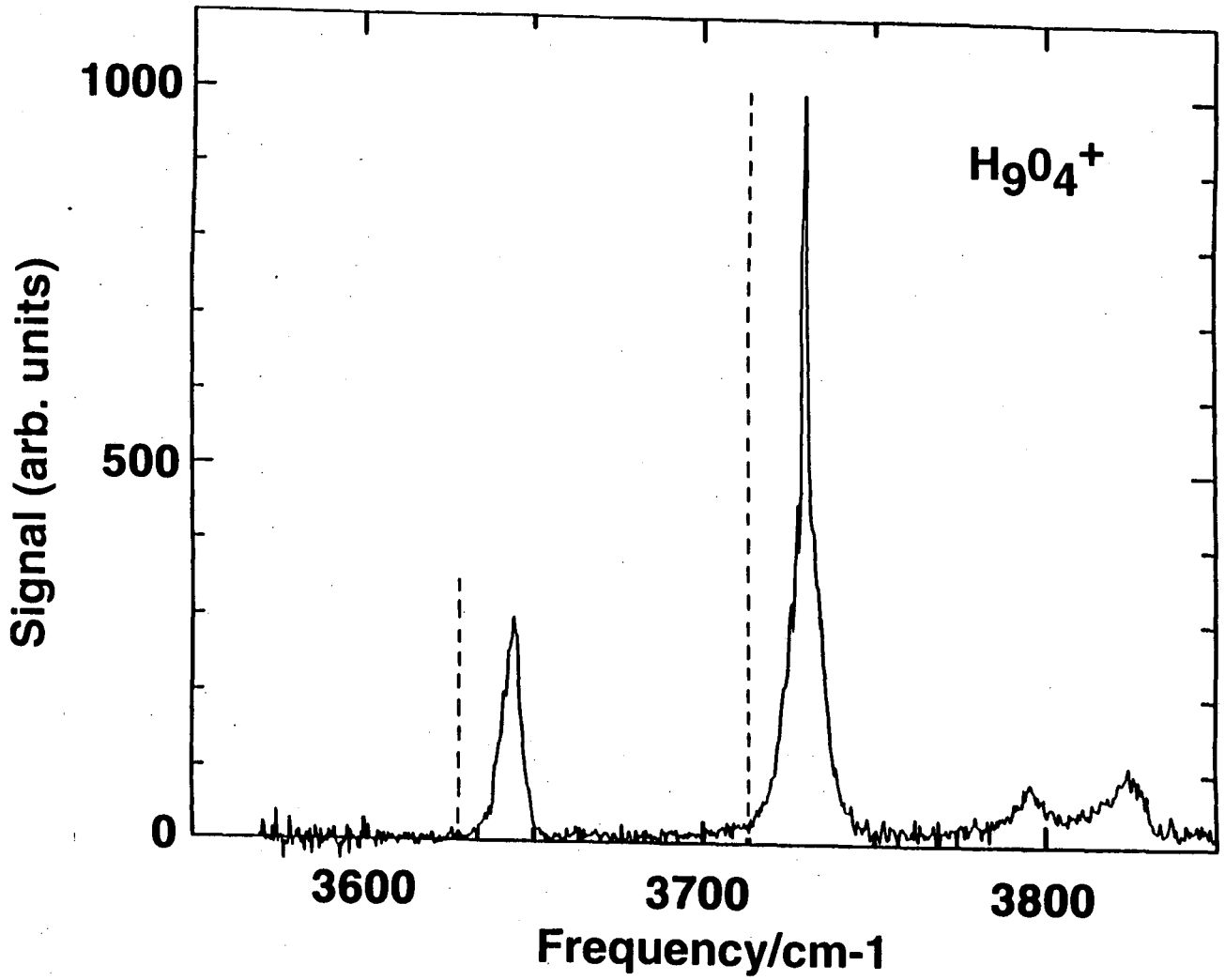
1000
500
0
Signal (arb. units)
$H_9O_4^+$
3600
3700
3800
Frequency/cm-1

Fig. 3

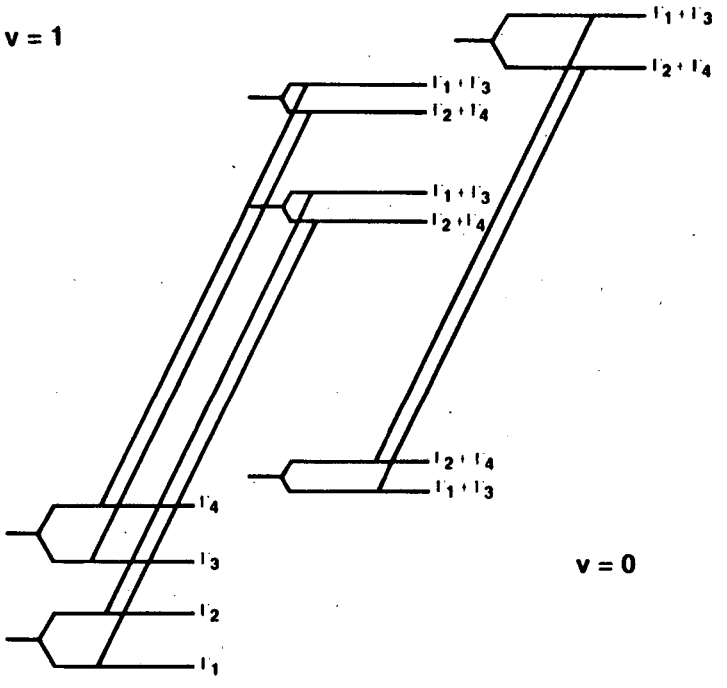


**Splitting Patterns:**

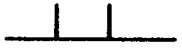

Fig. 4

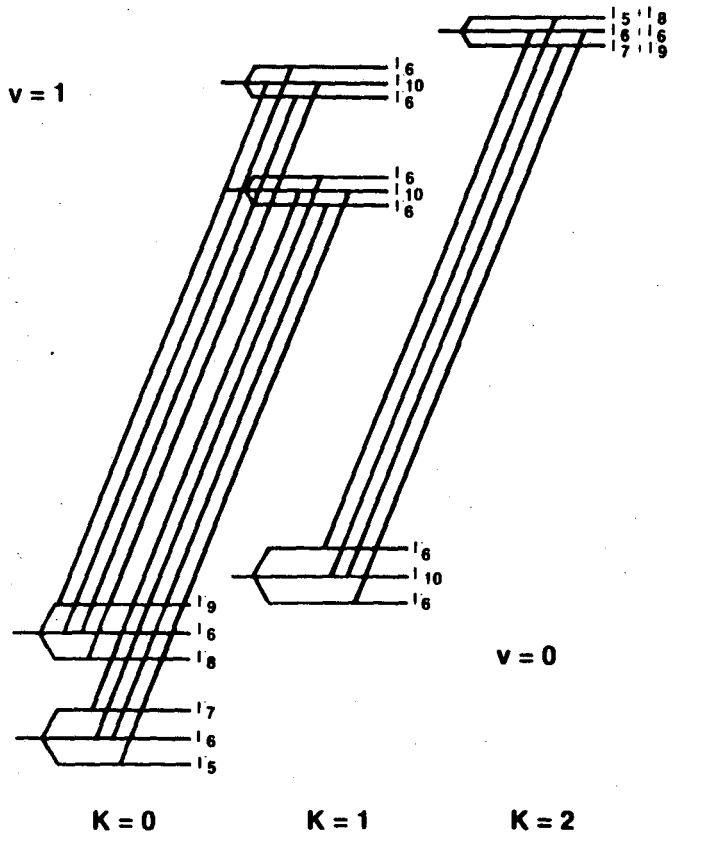


Fig. 5

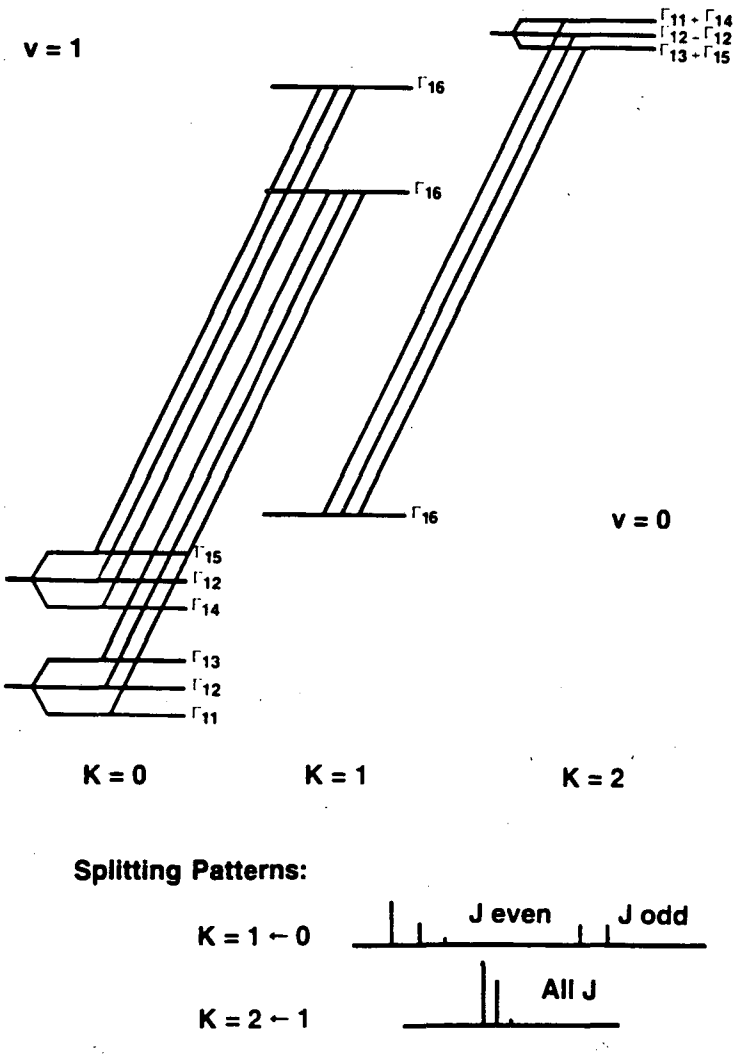
v = 1
Γ16
Γ16
Γ16
v = 0
Γ11 + Γ14
Γ12 - Γ12
Γ13 + Γ15
Γ15
Γ12
Γ14
Γ13
Γ12
Γ11
K = 0
K = 1
K = 2
Splitting Patterns:
K = 1 ← 0
J even
J odd
K = 2 ← 1
All J

Fig. 6

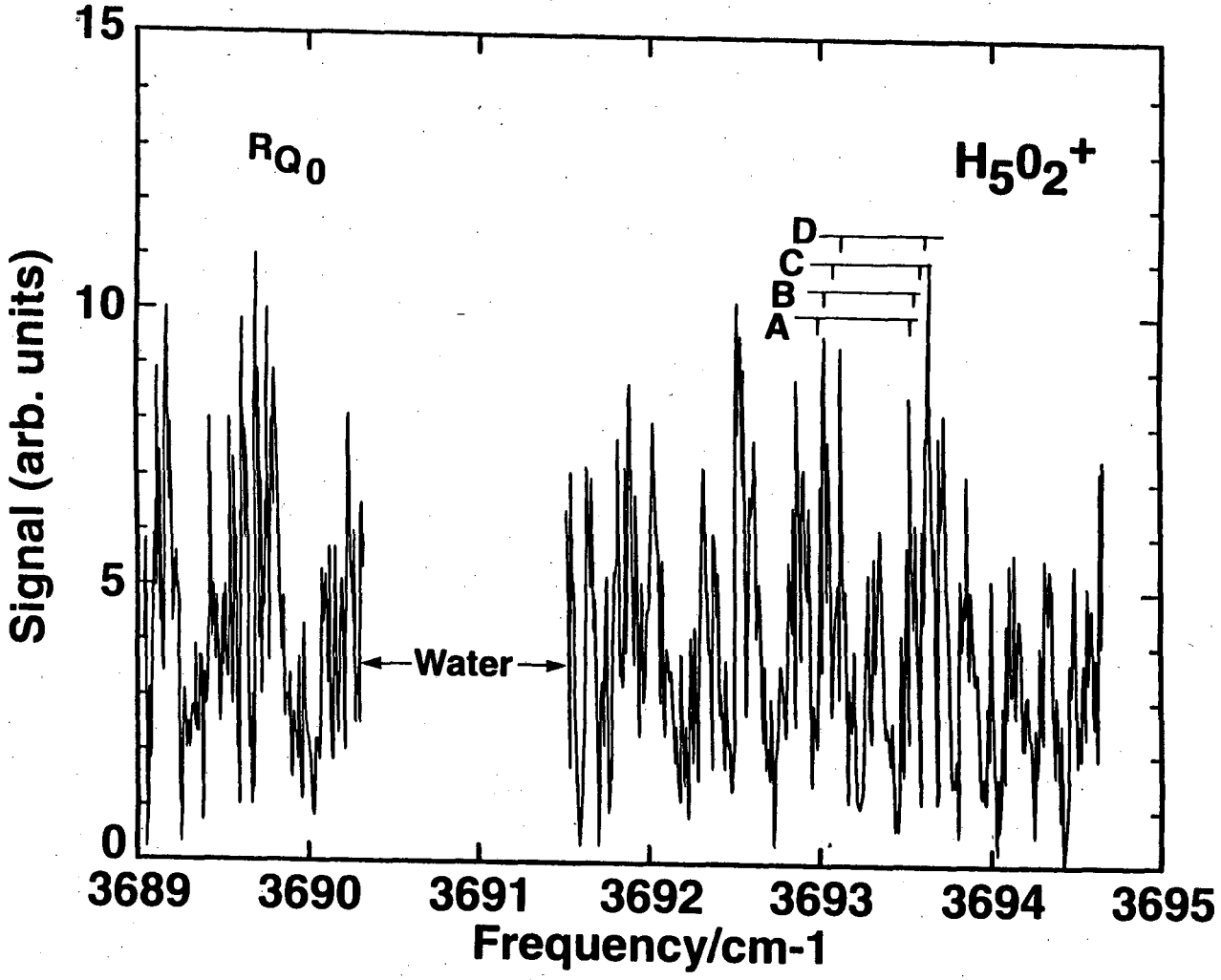
15
10
5
0
Signal (arb. units)
$^{R}Q_0$
$H_5O_2^+$
D
C
B
A
Water
3689
3690
3691
3692
3693
3694
3695
Frequency/cm-1

Fig. 7

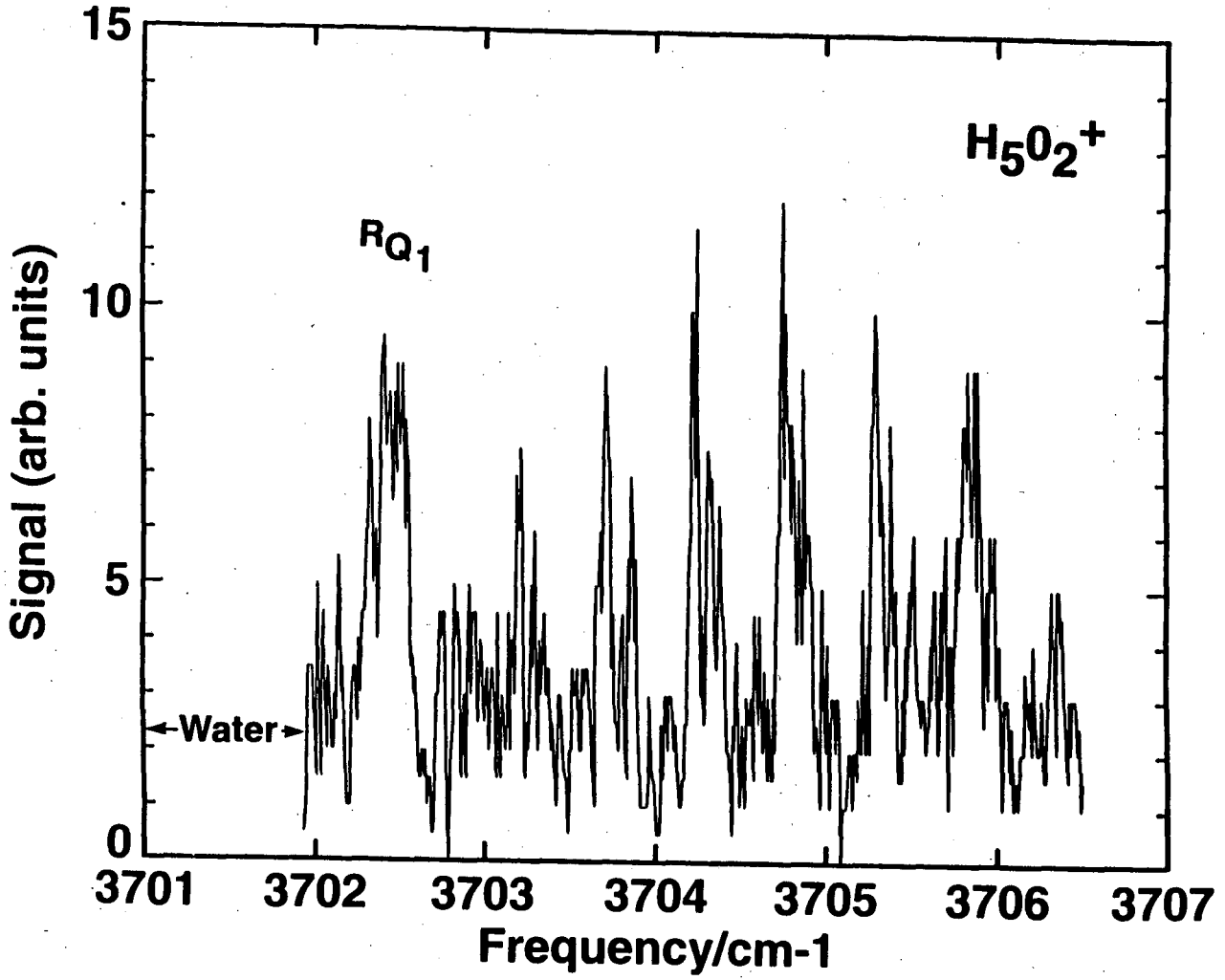
15
10
5
0
Signal (arb. units)
$H_5O_2^+$
$^RQ_1$
Water
3701
3702
3703
3704
3705
3706
3707
Frequency/cm-1

Fig. 8

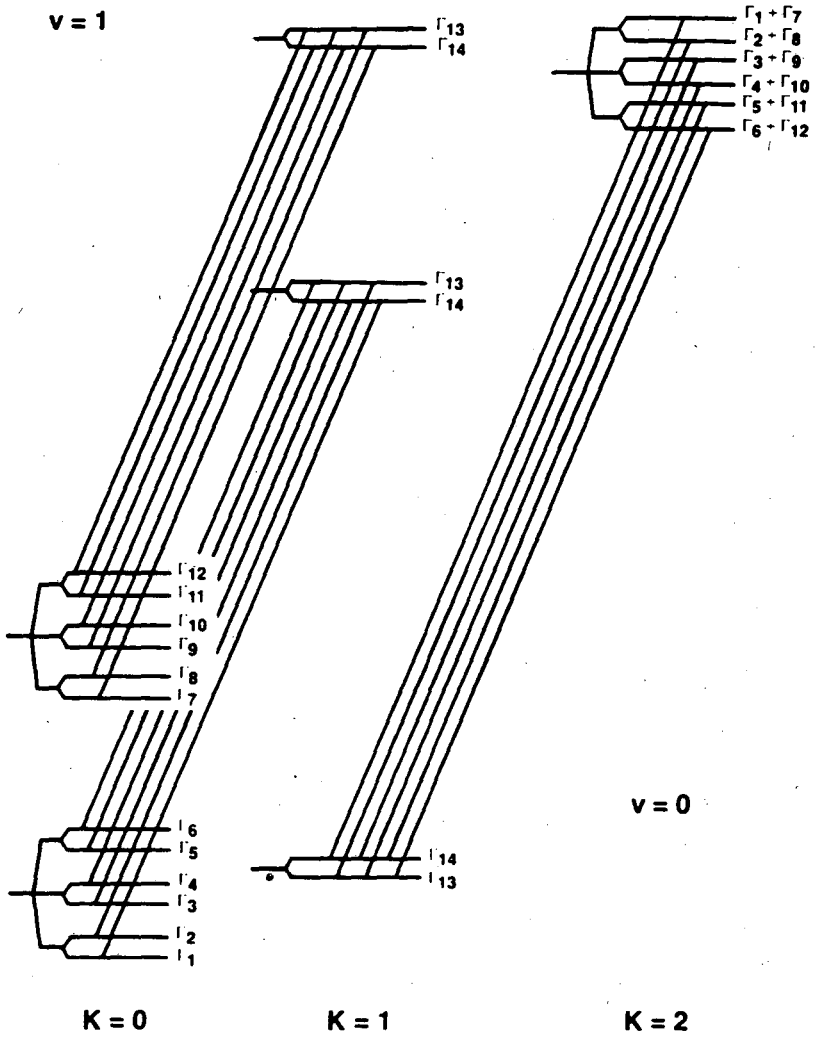


**Splitting Patterns:**

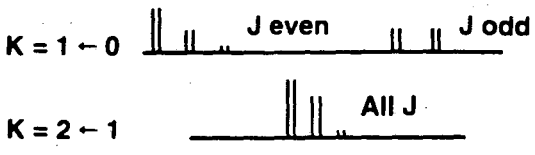


Fig. 9

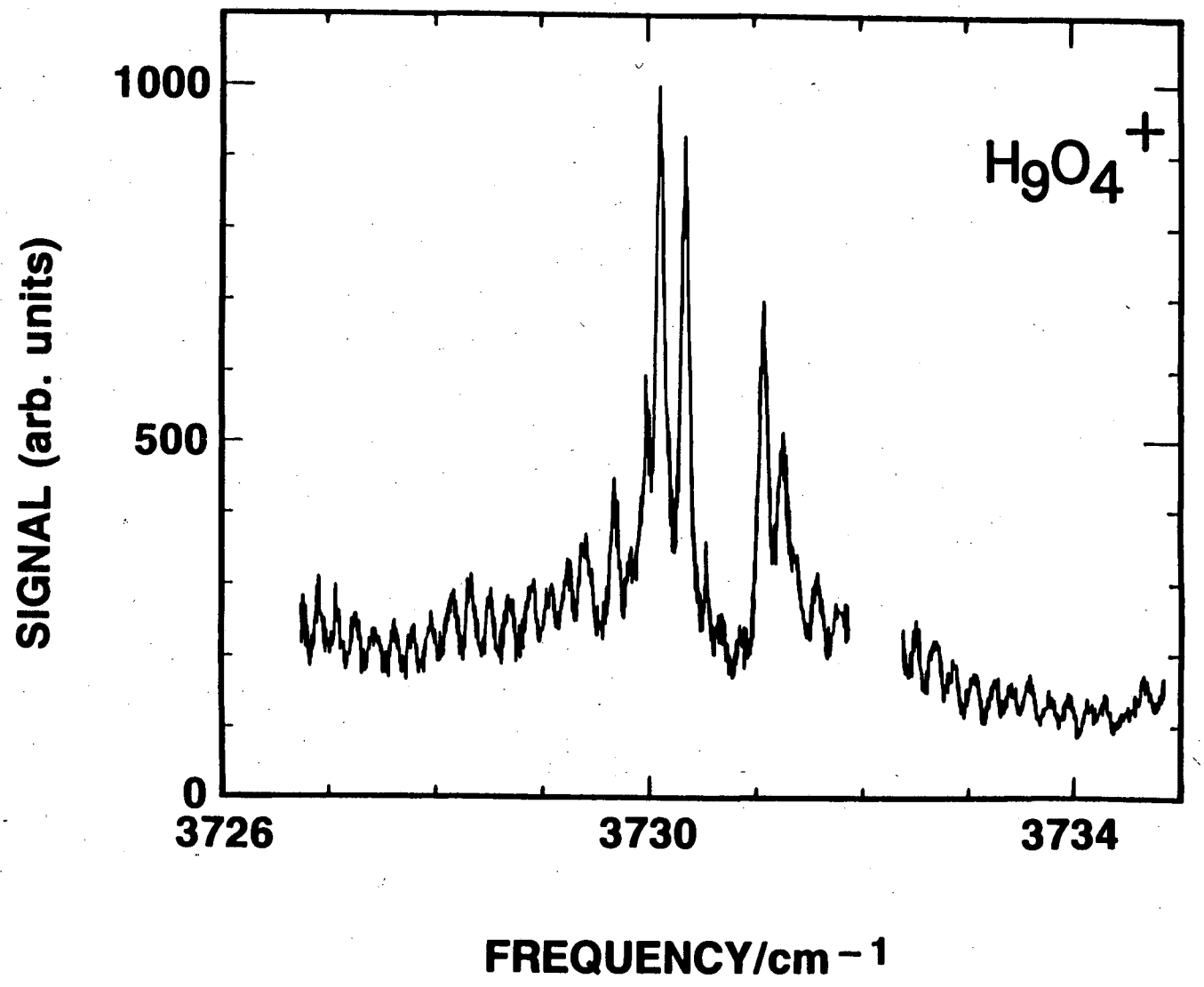
1000
500
0
SIGNAL (arb. units)
$H_9O_4^+$
3726
3730
3734
FREQUENCY/cm$^{-1}$

Fig. 10

LAWRENCE BERKELEY LABORATORY
UNIVERSITY OF CALIFORNIA
TECHNICAL INFORMATION DEPARTMENT
BERKELEY, CALIFORNIA 94720